



Published in final edited form as:

*Mol Psychiatry*. 2016 September ; 21(9): 1257–1262. doi:10.1038/mp.2015.160.

## Memory impairment in aged primates is associated with region-specific network dysfunction

Alexander Thomé, Ph.D.<sup>1,2</sup>, Daniel T. Gray, B.S.<sup>1,2</sup>, Cynthia A. Erickson, Ph.D.<sup>1,3</sup>, Peter Lipa, Ph.D.<sup>1,2</sup>, and Carol A. Barnes, Ph.D.<sup>1,2,4</sup>

<sup>1</sup>Evelyn F. McKnight Brain Institute, University of Arizona, Tucson, AZ

<sup>2</sup>ARL Division of Neural Systems, Memory & Aging, University of Arizona, Tucson, AZ

<sup>3</sup>Department of Psychology, Metropolitan State University of Denver, Denver, CO

<sup>4</sup>Departments of Psychology, Neurology, and Neuroscience, University of Arizona, Tucson, AZ

### Abstract

Age-related deficits in episodic memory result, in part, from declines in the integrity of medial temporal lobe structures, such as the hippocampus, but are not thought to be due to widespread loss of principal neurons. Studies in rodents suggest, however, that inhibitory interneurons may be particularly vulnerable in advanced age. Optimal encoding and retrieval of information depend on a balance of excitatory and inhibitory transmission. It is not known whether a disruption of this balance is observed in aging nonhuman primates, and whether such changes affect network function and behavior. To examine this question we combine large scale electrophysiological recordings with cell type-specific imaging in the medial temporal lobe of cognitively-assessed, aged rhesus macaques. We found that neuron excitability in hippocampal region CA3 is negatively correlated with the density of the somatostatin-expressing inhibitory interneurons in the vicinity of the recording electrodes in stratum oriens. By contrast, no hyperexcitability or interneuron loss was observed in the perirhinal cortex of these aged, memory-impaired monkeys. These data provide a link, for the first time, between selective increases in principal cell excitability and declines in a molecularly-defined population of interneurons that regulate network inhibition.

### Introduction

Senescence is associated with a number of changes in an organism's physiology and cognition. While only 14% of people over the age of 70 present with dementing neurological illnesses<sup>1</sup>, age-related memory impairments independent of dementia are common<sup>2</sup>. These normal age-related memory deficits can reduce quality of life, making it essential to understand their origin. Non-human primate models of aging are particularly powerful, as these animals also show age-related changes across a number of cognitive domains, but do

Users may view, print, copy, and download text and data-mine the content in such documents, for the purposes of academic research, subject always to the full Conditions of use:[http://www.nature.com/authors/editorial\\_policies/license.html#terms](http://www.nature.com/authors/editorial_policies/license.html#terms)

Correspondence to: Carol A. Barnes, Evelyn F. McKnight Brain Institute, University of Arizona, Life Sciences North, Rm 362, Tucson, AZ 85724-5115, (520) 626-2616, (520) 626-2618 FAX, carol@nsma.arizona.edu.

**Conflict of Interest:** The authors declare no competing financial interests.

not develop dementing disorders, providing the opportunity to study the cellular and molecular basis of these memory impairments in the absence of such diseases.

While several types of memory (e.g., recognition<sup>3</sup> and episodic<sup>4</sup> decline in normal aging, the brain structures that support these behaviors do not show significant reductions in principal cell numbers<sup>5-7</sup>. Among the clues to the biological mechanisms that may underlie these memory changes include separate studies showing that memory loss in rodents is associated with increased firing rates and disrupted spatial tuning in CA3<sup>8</sup>, declines in one population of GABAergic interneurons in that region<sup>9</sup>, and from fMRI studies that indicate hyperexcitability in the hippocampus of aged individuals<sup>10</sup>. Combined, these results suggest that a disruption of normal interactions between excitatory principal cells and inhibitory interneurons contribute to age-related memory impairments. To date, no studies exist that explicitly link behavioral changes to alterations in network activity and interneuron density in the same cohort of nonhuman primates. Towards this end, we performed multiple single-neuron recordings and immunohistochemical analyses for subtypes of GABAergic interneurons in behaviorally characterized middle-aged and senescent rhesus macaques.

## Materials and Methods

### Subjects

The data in the present study were collected from 5 male and female rhesus macaques (*Macacca mulatta*) ranging from middle age (13.5 (M), 15.4 (F), and 18.0 (F) years) to senescent (29.6 (M) and 31.7 (F) years). Human equivalent ages for these animals is 42 to 96 years<sup>11</sup>. All subjects were housed at the California National Primate Research Center in Davis, CA, where they participated in a long-term behavioral and electrophysiological study. The procedures described below were approved by the IACUC at the University of California, Davis, CA.

### Behavioral testing procedure

A modified Wisconsin General Test Apparatus (WGTA)<sup>12</sup> was used for the behavioral testing. The five animals performed a delayed nonmatching-to-sample (DNMS) task to assess their recognition memory. Previous studies have shown that performance on the DNMS task declines with age<sup>5,13-15</sup>. In addition, lesions of the hippocampus, perirhinal cortex, and inferior temporal cortex impair performance on the DNMS task<sup>16-20</sup>. Although the precise contributions that these individual temporal lobe structures make to the performance on this task continue to be discussed<sup>e.g.,21</sup>, it is clear that these systems normally cooperate in the production of this behavior<sup>22</sup>.

Each trial was initiated by a single object being placed over the center well that was baited with food reward. After the animal displaced the object and obtained the food reward, the stimulus was hidden from the animal's view for either 10, 15, 30, 60, 120, or 600 seconds. Following the delay, the initial object was presented over one of the lateral wells and a novel object was placed over the other lateral (now baited) well. Animals were allowed a single response, and were only rewarded if they first displaced the novel object. Novel object pairs were used in every trial and reward items were placed over the left and right lateral wells

with equal frequency. Monkeys were tested for 20 trials per day for 5 days a week for all delays except the 10 min delay in which 5 trials per day were given over 10 days.

### **Procedures for headpost attachment and electrode implantation**

Procedures for implantation of headposts and the chronic implantation of hyperdrives are as described elsewhere in more detail<sup>23,24</sup>. Briefly, all animals received pre-surgical structural MRIs from which individual stereotaxic coordinates for electrode placement were calculated to coincide with the location of the middle of the hippocampus (as can be viewed in Plate 68<sup>25</sup>). Hyperdrives consisted of 14 threaded manipulator legs, 12 of which independently moved our custom manufactured tetrode recording probes<sup>23</sup> with one serving as a moveable reference electrode, and one as ground.

### **Single Unit Data Acquisition**

The single unit data obtained from the 12 tetrode recording probes were sampled at 32 kHz, using the Neuralynx Cheetah data acquisition system (Neuralynx, Bozeman, MT). The multiple single cells were separated and identified offline using either XClust (M.A. Wilson) or MClust (A.D. Redish). Electrodes were only moved at the end of a day's recording session. The criteria for inclusion included that neurons were well-isolated and stable throughout the entire recording period. Firing rates were calculated as the inverse of the mean of the inter-spike interval. All data analysis was performed using custom scripts written in MATLAB (The Mathworks, Inc., Cambridge MA).

### **Histological Processing and Antibody Characterization**

Animals were euthanized with an overdose of sodium pentobarbital (60 mg/kg, i.v.), and transcardially perfused with a solution of 4% paraformaldehyde in 0.01% phosphate buffer saline (PBS; pH 7.4) followed by a mixture of 4% paraformaldehyde and 10% sucrose. After perfusion, the brains were extracted and placed in a solution of 4% paraformaldehyde and 30% sucrose for further cryoprotection. All brains were cut transversely at 30 $\mu$ m. Tissue sections adjacent to tetrode recording probe locations in the CA3 region of the hippocampus and the perirhinal cortex were immunohistochemically stained for glutamic acid decarboxylase-67 (GAD 67), parvalbumin (PV) or somatostatin (SOM).

The sections were blocked for 24 hours in 3% normal horse serum (Vector Laboratories, Burlingame, CA; S-2000) and 0.25% Triton X (Sigma-Aldrich, St. Louis, MO; x100), followed by a 24 hour incubation in a solution containing a mixture of either the primary PV antibody (anti-PV in mouse, 1:2000; Sigma-Aldrich; p3088) or primary SOM antibody (anti-SOM in mouse, 1:350; Santa Cruz Biotechnology, Dallas, TX; 74556) along with the primary GAD67 antibody (anti-GAD1 in Rabbit; 1:1000, Sigma-Aldrich; SAB4501075). Following this incubation the sections underwent three 15 minute washes in 0.01% PBS. The sections were then incubated for 48 hours in a solution containing two secondary fluorescent antibodies of different emission wavelengths, one specific to mouse IgG (Alexa Fluor 594; 1:250; Life Technologies Grand Island, NY; A21206) and the other specific to rabbit IgG (Alexa Fluor 488; 1:250; Life Technologies,; A21203). Following three more 15-minute rinses in PBS the sections were mounted with a vectashield fluorescent mounting

medium containing the nuclear marker DAPI (Vector Laboratories; H1200), cover-slipped, and imaged.

Isotype specificities for all of the primary antibodies were tested by the manufacturers with a variety of tests. A double diffusion immunoassay with mouse monoclonal antibody isotyping reagents (Sigma-Aldrich; ISO-2) validated the specificity of the anti-PV antibody. Western blot analyses of both the SOM and GAD antibodies yielded single bands when blotted on whole cell lysates from human (SOM) and rodent (GAD) tissue.

### Quantification of Immunohistochemically-defined interneurons

All images were acquired using a 10x air objective on a DeltaVision RT Deconvolution Microscope. DAPI nuclear staining was used to identify the hippocampal CA3, CA1 and dentate gyrus hilar regions as well as the perirhinal cortex (PRC). Borders for the CA3, CA1, dentate hilus and perirhinal cortex were drawn in accordance with the Paxinos et al.<sup>25</sup> rhesus macaque brain atlas. For every section we acquired large panel images in different fluorescent filters to visualize PV/SOM, GAD67 and DAPI. Each panel contained all four regions of interest. To avoid biases from fragmented cells at the edges of the tissue, a consistent 5  $\mu\text{m}$  guard space on either side of the z-plane was used to scan the depth of the tissue<sup>26,27</sup>. The guard space was implemented by manually finding the top and bottom edges of the tissue with the microscope and beginning the image collection in the z-plane 5  $\mu\text{m}$  from the top edge and terminating it 5  $\mu\text{m}$  from the bottom edge. Images were acquired in 3  $\mu\text{m}$  steps in the z-plane. Images were imported into Adobe Photoshop CS5 (Adobe Systems Inc., San Jose, CA) where they were line averaged, co-registered and collapsed across the z-plane to yield a single 2D image. All sections were assigned random identifiers to ensure the two counters were blind to the experimental condition.

The goal of the immunohistochemical analysis was not to stereologically quantify the number of PV and SOM interneurons across the hippocampus, but rather to obtain local estimates of interneuron density surrounding the tetrode locations from which we obtained single unit recordings from each animal. To obtain these local estimates of interneuron density, brain sections immediately adjacent (both anterior and posterior) to brain sections with electrode tracks were prepared for immunofluorescent analysis. Since the exact anterior-posterior location of recording sites differed between animals, unbiased sampling was not possible, thus eliminating the application of full stereological analysis. This method, however, did allow us to obtain local estimates of neuron density with respect to electrode recording sites.

Neuron numbers were quantified by placing counting grids (the size of each counting square was 200  $\mu\text{m}$  \*200 $\mu\text{m}$ ) within the defined borders of the CA3, CA1, dentate gyrus hilus and PRC lamina. In the CA3 and CA1, PV and SOM interneurons were found most consistently in the stratum oriens and to a lesser extent, but also consistently in stratum radiatum; hence interneurons were sampled separately from these two layers. In the PRC, interneurons were sampled from the deep and superficial layers. For each animal we stained a total of 8 sections, 4 stained for SOM and 4 stained for PV, half of these sections used for SOM and PV stains were anterior to recording sites and the other half were posterior to the recording sites. To estimate the interneuron density around the recording sites, four counting grids

were placed in each lamina from each region, and neurons falling within the borders of the grids were counted. Neurons that partially entered the counting field were counted if they touched one of two randomly selected sides of the area and excluded if they touched the other two. In total, every animal contributed exactly the same amount of sampling area to the analysis, ensuring that no single animal contributed disproportionately to the age comparison. We acquired 16 samples per interneuron type in every layer per animal. To avoid confounds due to changes in the local density associated with transition zones between different regions, samples were obtained well away from these boundaries.

The counts from all sections within a region were averaged for each animal, producing one value per lamina, per region, per stain, per animal. As we predicted *a priori* that the change in firing rates in old animals is due to a loss of inhibitory interneurons within a specific lamina, we performed a 1-tailed t-test to test the hypothesis that there are fewer interneurons in the aged animals compared to young. To verify counting accuracy, a subset (20%) of images were counted a second time by an independent rater. Inter-rater reliability was high ( $r = .92$ ,  $p < .00001$  Pearson correlation).

## Results

Compared to middle-aged animals, senescent animals performed worse on a delayed nonmatching-to-sample (DNMS) task, which is in part dependent on integrity of medial temporal lobe structures<sup>28</sup>. Older monkeys were impaired at the longest delay interval (600 second delay condition,  $t(3) = -5.12$ ,  $p = 0.02$ ;  $\text{Mean}_{\text{MA}} = 82\%$ ;  $\text{Mean}_{\text{SN}} = 59\%$ , Figure 1A). The absence of differences at the very short delays (10 and 15 sec) likely rules out contributions from a number of other non-cognitive factors (e.g., vision problems due to macular degeneration or motivational differences).

To test whether these deficits were associated with changes in network function, we recorded the activity of 662 well-isolated single units from the CA3 region of the hippocampus and the perirhinal cortex (PRC). For CA3, these data came from 2 young and 2 old animals (we did not isolate CA3 cells from one of the young animals); for PRC, the data came from 3 young and 2 old animals. As our primary variable of interest was basal excitability of principal cells, we confined our analysis to the pre-experimental rest epoch in which primates sat quietly in a sound-attenuating chamber. Principal cells were separated from putative fast-spiking interneurons by their waveform characteristics (Figure 1B)<sup>29,30</sup>. While this approach cannot identify interneuron types that possess waveforms similar to those of principal cells, it does eliminate a possible confound due to inadvertent inclusion of fast spiking interneurons that would bias estimates of population firing rate. Too few putative fast-spiking interneurons were encountered for valid age comparisons.

Baseline firing rates in CA3, but not PRC, were significantly higher in senescent than younger monkeys (CA3:  $W = 11640$ ,  $p < 0.00001$ ; PRC:  $W = 6121$ ,  $p > 0.17$ ; Wilcoxon Rank Sum test). The median firing rates for neurons in MA and SN animals were: 0.05 Hz (MA  $n = 152$ ) versus 0.18 Hz (SN  $n = 273$ ) in CA3 and 0.49 Hz (MA  $n = 138$ ) versus 0.51 Hz (SN  $n = 99$ ) in the PRC (Figure 1C). To ensure that the effects were not due to overweighting of neurons from a single animal we also compared the median firing rates per animal. Again

the firing rates were higher for SN relative to MA animals in CA3 ( $t(2) = 4.13$ ,  $p = 0.027$ ;  $\text{Mean}_{\text{MA}} = 0.03$  Hz;  $\text{Mean}_{\text{SN}} = 0.22$  Hz, Cohen's  $d = 3.94$ ), but not in the PRC ( $t(2) = 0.45$ ,  $p = 0.35$ ;  $\text{Mean}_{\text{MA}} = 0.37$  Hz;  $\text{Mean}_{\text{SN}} = 0.66$  Hz, Cohen's  $d = 0.46$ ).

Next, using immunohistochemistry, we examined whether the changes in firing rate are linked to the composition of populations of inhibitory interneurons in these regions. Immunofluorescent staining for parvalbumin and somatostatin was performed on postmortem tissue sections located immediately adjacent to electrode tracks (Figure 2A). For this analysis, we included the adjacent CA1 region and the hilar region of the dentate gyrus (which we did not target for recordings), to determine whether the observed changes were specific to the CA3 region or were seen across hippocampal subregions. Parvalbumin and somatostatin neurons in the CA1, CA3 and hilar regions of the hippocampus as well as PRC were co-registered with glutamic acid decarboxylase 67 (GAD67) immunoreactivity (Figure 2B) and counterstained with DAPI. The background staining of our GAD antibody was too high to reliably discriminate punctate cell bodies for quantification; however GAD67 did serve as a useful marker to confirm the GABAergic profile of the interneurons.

Cells expressing positive label for somatostatin or parvalbumin and GAD67 antibodies were counted in middle-aged and senescent monkeys. There was a significant age-related decrease in somatostatin interneurons in the stratum oriens of both the CA1 and CA3 region (CA1:  $t(3) = 2.78$ ,  $p < 0.04$ ,  $\text{Mean}_{\text{CA1-MA}} = 8$ ,  $\text{Mean}_{\text{CA1-SN}} = 6.34$ ; CA3:  $t(3) = 2.49$ ,  $p < 0.04$ ,  $\text{Mean}_{\text{CA3-MA}} = 9.54$ ,  $\text{Mean}_{\text{CA3-SN}} = 7.5$ , Figure 2D). We observed no significant changes in the stratum radiatum of either CA1 or CA3, nor in any population of parvalbumin containing interneurons in those region (Figure 2C, E). Similarly, we observed no changes in the density of either somatostatin or parvalbumin neurons in the hilus of the dentate gyrus, or in the superficial or deep layers of the perirhinal cortex (Figure 2E, F, summary statistics for all regions in Table 1). Thus, the dissociation at the regional, laminar and cell-type level make it unlikely that these results would have arisen from counting biases or a change in the quality of tissue from aged animals.

To understand the relationship between interneuron cell counts, principal cell firing rates in the CA3 region and performance on the DNMS task, we performed a series of linear regressions. The density of somatostatin interneurons in the stratum oriens of CA3 was significantly correlated with firing rate ( $r^2 = 0.91$ ,  $F(1,2) = 22.76$ ,  $p = 0.04$ , linear regression, Figure 3A). Unfortunately, the small animal sample size, limits our ability to reliably assess further interactions between behavior and changes in firing rate and cell counts. We present these correlations in Figure 3 (B, C, respectively), as the trend in these data is consistent with the idea that these factors may be related to deficits in behavioral performance.

## Discussion

The primary novel finding in the present study is that hyperexcitability of aged hippocampal CA3 pyramidal cells is associated with reduced numbers of somatostatin (SOM)-positive interneurons in memory-impaired older monkeys. This decline in somatostatin interneurons was region-specific (CA3 and CA1, not in the hilar region of the dentate gyrus or in perirhinal cortex, PRC), laminar-specific (stratum oriens, not radiatum), and interneuron-

selective (no change in parvalbumin interneurons). The observed reduction in SOM interneurons could either reflect cell loss or a change in phenotype<sup>31</sup>, however, these data do not allow conclusive differentiation between these possibilities.

The hippocampus stores information via a distributed population code, with episodes represented as orthogonal patterns of activity. Inhibitory interneurons in the hippocampus are believed to sample the same synaptic input received by principal neurons, enabling them to dynamically regulate the overall excitability of the network<sup>32,33</sup>. A failure of interneurons to properly regulate network activity could result in high firing rates and more broadly-tuned neuronal responses. This could lead to large amounts of overlap between competing representations, resulting in retrieval errors. Given the hierarchical and reciprocal organization of the medial temporal lobe memory system<sup>34</sup>, corrupted information may spread through the system, amplifying the error and decreasing performance.

Consistent with the interpretation of impaired representations in the hippocampus, CA3 neurons in aged rodents show decreased spatial selectivity that is correlated with a decline in the ability to discriminate between two environments<sup>8</sup>. Similarly, older adults with impaired pattern separation abilities also show increased BOLD activity in CA3 and dentate gyrus regions in fMRI experiments<sup>35</sup>. Furthermore, normalizing this activity by administration of the anticonvulsant levetiracetam partially rescues cognitive performance in patients with mild cognitive impairment<sup>36</sup>. Our demonstration of age-related behavioral deficits associated with changes in network excitability and interneuron loss in the non-human primate bridges the gap between the aged human imaging data and cellular data in aging rodents.

Our data documenting a reduction in SOM interneuron counts in the stratum oriens of the CA1 region may appear to be at odds with data from physiological studies in rodents<sup>e.g.,37</sup> and functional imaging data in humans<sup>e.g.,35</sup> that show no evidence of an increase in basal excitability in this region. We believe this could be explained in part by increased afterhyperpolarizing potentials (AHPs) in principal neurons in the CA1 region in aging<sup>38</sup>. By effectively increasing the refractory period of neurons, the increased AHP may limit excitability increases in CA1. While no studies to date have examined AHPs in CA1 pyramidal cells of nonhuman primates, superficial layer dorsolateral prefrontal cortical cells do show increased AHP amplitudes in the macaque<sup>39</sup>. Future studies of AHPs in CA1 of primates could confirm the hypothesis that the effect of the loss of SOM interneurons may be balanced by excitability decreases produced by larger amplitude AHPs. Additionally, our study finds no changes in interneuron density in the hilus of the dentate gyrus in contrast to histological studies in rodents<sup>e.g.,40</sup>. Future studies are needed to confirm this difference in the pattern of age-related interneuron loss between primates and rodents.

While many cellular characteristics remain stable across the lifespan, a number of distinct changes occur that may interact with the altered GABAergic tone reported here. These include region-specific loss of synaptic contacts<sup>41</sup>, reduced synaptic plasticity<sup>42</sup>, decreased cholinergic function<sup>43,44</sup> and altered gene expression<sup>45,46</sup>. Hyperexcitability (as observed in CA3) has also been observed in primary sensory systems of senescent primates<sup>47</sup>, although other cortical regions do not exhibit activity increases. In fact, neurons in the prefrontal

cortex of aged animals show reduced firing rates during the delay period of a spatial working memory task<sup>48</sup>. The interregional variability in the sign of these changes highlights the fact that therapies aimed at restoring optimal performance in aging brains must be highly selective. Our data suggest that rebalancing local network excitability in regions vulnerable to the aging process may be a productive avenue in treatment of age-related cognitive decline<sup>49</sup>. In the case of CA3, one target appears to be lamina-specific changes in GABAergic transmission linked to somatostatin-containing interneurons.

## Acknowledgments

This work was supported by AG003376, McKnight Brain Research Foundation and CNPRC Center grant RR000169. The authors would like to thank Bruce McNaughton for help with the design of the primate hyperdrive and participation in the implant surgeries. We also thank Katalin Gothard for participation in all headpost surgeries for the animals, Bill Skaggs, Michele Permenter, Julie Vogt, and Matthew Archibeque for acquisition of the single unit data, Jie Wang for cell separation and processing the single unit data. We thank Alison Comrie and Chelsea Takamatsu for help with the immunohistochemistry image processing, and we are also grateful to Rachel Samson for consultation on statistical analyses. AT is currently at the Department of Brain and Cognitive Sciences, University of Rochester; Rochester, NY.

## References

1. Plassman BL, Langa KM, Fisher GG, Heeringa SG, Weir DR, Ofstedal MB, et al. Prevalence of Dementia in the United States: The Aging, Demographics, and Memory Study. *Neuroepidemiology*. 2007; 29:125–132. [PubMed: 17975326]
2. Luo L, Craik F. Aging and memory: A cognitive approach. *Can J Psychiatry Rev Can Psychiatr*. 2008; 53:346–353.
3. Burke SN, Ryan L, Barnes CA. Characterizing cognitive aging of recognition memory and related processes in animal models and in humans. *Front Aging Neurosci*. 2012; 4:15. [PubMed: 22988437]
4. Moscovitch M, Nadel L, Winocur G, Gilboa A, Rosenbaum RS. The cognitive neuroscience of remote episodic, semantic and spatial memory. *Curr Opin Neurobiol*. 2006; 16:179–190. [PubMed: 16564688]
5. Rapp PR, Amaral DG. Evidence for task-dependent memory dysfunction in the aged monkey. *J Neurosci Off J Soc Neurosci*. 1989; 9:3568–3576.
6. West MJ, Coleman PD, Flood DG, Troncoso JC. Differences in the pattern of hippocampal neuronal loss in normal ageing and Alzheimer's disease. *Lancet*. 1994; 344:769–772. [PubMed: 7916070]
7. Kecker JIH, Luiten PGM, Fuchs E. Preservation of hippocampal neuron numbers in aged rhesus monkeys. *Neurobiol Aging*. 2003; 24:157–165. [PubMed: 12493561]
8. Wilson IA, Ikonen S, Gallagher M, Eichenbaum H, Tanila H. Age-Associated Alterations of Hippocampal Place Cells Are Subregion Specific. *J Neurosci*. 2005; 25:6877–6886. [PubMed: 16033897]
9. Spiegel AM, Koh MT, Vogt NM, Rapp PR, Gallagher M. Hilar interneuron vulnerability distinguishes aged rats with memory impairment. *J Comp Neurol*. 2013:n/a–n/a.
10. Mitchell KJ, Johnson MK, Raye CL, D'Esposito M. fMRI evidence of age-related hippocampal dysfunction in feature binding in working memory. *Brain Res Cogn Brain Res*. 2000; 10:197–206. [PubMed: 10978709]
11. Tigges J, Gordon TP, McClure HM, Hall EC, Peters A. Survival rate and life span of rhesus monkeys at the Yerkes Regional Primate Research Center. *Am J Primatol*. 1988; 15:263–273.
12. Harlow H, Bromer J. A test apparatus for monkeys. *Psychol Rec*. 1938
13. Moss MB, Rosene DL, Peters A. Effects of aging on visual recognition memory in the rhesus monkey. *Neurobiol Aging*. 1988; 9:495–502. [PubMed: 3062461]
14. Herndon JG, Moss MB, Rosene DL, Killiany RJ. Patterns of cognitive decline in aged rhesus monkeys. *Behav Brain Res*. 1997; 87:25–34. [PubMed: 9331471]

15. Alexander GE, Chen K, Aschenbrenner M, Merkle TL, Santerre-Lemmon LE, Shamy JL, et al. Age-Related Regional Network of Magnetic Resonance Imaging Gray Matter in the Rhesus Macaque. *J Neurosci*. 2008; 28:2710–2718. [PubMed: 18337400]
16. Mishkin M. Memory in monkeys severely impaired by combined but not by separate removal of amygdala and hippocampus. *Nature*. 1978; 273:297–298. [PubMed: 418358]
17. Murray EA, Mishkin M. Severe tactual as well as visual memory deficits follow combined removal of the amygdala and hippocampus in monkeys. *J Neurosci Off J Soc Neurosci*. 1984; 4:2565–2580.
18. Saunders RC, Murray EA, Mishkin M. Further evidence that amygdala and hippocampus contribute equally to recognition memory. *Neuropsychologia*. 1984; 22:785–796. [PubMed: 6527768]
19. Buffalo EA, Ramus SJ, Squire LR, Zola SM. Perception and Recognition Memory in Monkeys Following Lesions of Area TE and Perirhinal Cortex. *Learn Mem*. 2000; 7:375–382. [PubMed: 11112796]
20. Zola SM, Squire LR, Teng E, Stefanacci L, Buffalo EA, Clark RE. Impaired Recognition Memory in Monkeys after Damage Limited to the Hippocampal Region. *J Neurosci*. 2000; 20:451–463. [PubMed: 10627621]
21. Baxter MG, Murray EA. Opposite relationship of hippocampal and rhinal cortex damage to delayed nonmatching-to-sample deficits in monkeys. *Hippocampus*. 2001; 11:61–71. [PubMed: 11261774]
22. Barker GRI, Warburton EC. When Is the Hippocampus Involved in Recognition Memory? *J Neurosci*. 2011; 31:10721–10731. [PubMed: 21775615]
23. Skaggs WE, McNaughton BL, Permenter M, Archibeque M, Vogt J, Amaral DG, et al. EEG sharp waves and sparse ensemble unit activity in the macaque hippocampus. *J Neurophysiol*. 2007; 98:898. [PubMed: 17522177]
24. Thome A, Erickson CA, Lipa P, Barnes CA. Differential effects of experience on tuning properties of macaque MTL neurons in a passive viewing task. *Hippocampus*. 2012; 22:2000–2011. [PubMed: 22987678]
25. Paxinos, G.; Huang, X-F.; Toga, AW. *The Rhesus Monkey Brain in Stereotaxic Coordinates*. 1. Academic Press; San Diego: 1999.
26. West MJ, Coleman PD, Flood DG, Troncoso JC. Differences in the pattern of hippocampal neuronal loss in normal ageing and Alzheimer's disease. *Lancet*. 1994; 344:769–772. [PubMed: 7916070]
27. Mouton PR, Gokhale AM, Ward NL, West MJ. Stereological length estimation using spherical probes. *J Microsc*. 2002; 206:54–64. [PubMed: 12000563]
28. Squire LR, Zola-Morgan S. The medial temporal lobe memory system. *Science*. 1991; 253:1380. [PubMed: 1896849]
29. Bartho P, Hirase H, Monconduit L, Zugaro M, Harris KD, Buzsáki G. Characterization of neocortical principal cells and interneurons by network interactions and extracellular features. *J Neurophysiol*. 2004; 92:600. [PubMed: 15056678]
30. Mitchell JF, Sundberg KA, Reynolds JH. Differential Attention-Dependent Response Modulation across Cell Classes in Macaque Visual Area V4. *Neuron*. 2007; 55:131–141. [PubMed: 17610822]
31. Stanley DP, Shetty AK. Aging in the rat hippocampus is associated with widespread reductions in the number of glutamate decarboxylase-67 positive interneurons but not interneuron degeneration. *J Neurochem*. 2004; 89:204–216. [PubMed: 15030405]
32. McNaughton BL, Morris RGM. Hippocampal synaptic enhancement and information storage within a distributed memory system. *Trends Neurosci*. 1987; 10:408–415.
33. Freund TF, Buzsáki G. Interneurons of the hippocampus. *Hippocampus*. 1996; 6:347–470. [PubMed: 8915675]
34. Lavenex P, Amaral DG. Hippocampal-neocortical interaction: a hierarchy of associativity. *Hippocampus*. 2000; 10:420–430. [PubMed: 10985281]
35. Yassa MA, Lacy JW, Stark SM, Albert MS, Gallagher M, Stark CEL. Pattern separation deficits associated with increased hippocampal CA3 and dentate gyrus activity in nondemented older adults. *Hippocampus*. 2011; 21:968–979. [PubMed: 20865732]

36. Bakker A, Krauss GL, Albert MS, Speck CL, Jones LR, Stark CE, et al. Reduction of Hippocampal Hyperactivity Improves Cognition in Amnesic Mild Cognitive Impairment. *Neuron*. 2012; 74:467–474. [PubMed: 22578498]
37. Wilson IA, Ikonen S, Gallagher M, Eichenbaum H, Tanila H. Age-associated alterations of hippocampal place cells are subregion specific. *J Neurosci*. 2005; 25:6877–6886. [PubMed: 16033897]
38. Landfield PW, Pitler TA. Prolonged Ca<sup>2+</sup>-dependent afterhyperpolarizations in hippocampal neurons of aged rats. *Science*. 1984; 226:1089–1092. [PubMed: 6494926]
39. Luebke JI, Amatrudo JM. Age-related increase of sI(AHP) in prefrontal pyramidal cells of monkeys: relationship to cognition. *Neurobiol Aging*. 2012; 33:1085–1095. [PubMed: 20727620]
40. Stanley DP, Shetty AK. Aging in the rat hippocampus is associated with widespread reductions in the number of glutamate decarboxylase-67 positive interneurons but not interneuron degeneration. *J Neurochem*. 2004; 89:204–216. [PubMed: 15030405]
41. Geinisman Y, de Toledo-Morrell L, Morrell F, Persina IS, Rossi M. Age-related loss of axospinous synapses formed by two afferent systems in the rat dentate gyrus as revealed by the unbiased stereological dissector technique. *Hippocampus*. 1992; 2:437–444. [PubMed: 1308200]
42. Barnes CA. Memory deficits associated with senescence: A neurophysiological and behavioral study in the rat. *J Comp Physiol Psychol*. 1979; 93:74–104. [PubMed: 221551]
43. Bartus RT, Dean RL, Beer B, Lippa AS. The cholinergic hypothesis of geriatric memory dysfunction. *Science*. 1982; 217:408–414. [PubMed: 7046051]
44. Shen J, Barnes CA. Age-related decrease in cholinergic synaptic transmission in three hippocampal subfields. *Neurobiol Aging*. 1996; 17:439–451. [PubMed: 8725906]
45. Penner MR, Roth TL, Chawla MK, Hoang LT, Roth ED, Lubin FD, et al. Age-related changes in Arc transcription and DNA methylation within the hippocampus. *Neurobiol Aging*. 2011; 32:2198–2210. [PubMed: 20189687]
46. Berchtold NC, Coleman PD, Cribbs DH, Rogers J, Gillen DL, Cotman CW. Synaptic genes are extensively downregulated across multiple brain regions in normal human aging and Alzheimer's disease. *Neurobiol Aging*. 2013; 34:1653–1661. [PubMed: 23273601]
47. Juarez-Salinas DL, Engle JR, Navarro XO, Recanzone GH. Hierarchical and serial processing in the spatial auditory cortical pathway is degraded by natural aging. *J Neurosci Off J Soc Neurosci*. 2010; 30:14795–14804.
48. Wang M, Gamo NJ, Yang Y, Jin LE, Wang X-J, Laubach M, et al. Neuronal Basis of Age-Related Working Memory Decline. *Nature*. 2011; 476:210–213. [PubMed: 21796118]
49. Koh MT, Rosenzweig-Lipson S, Gallagher M. Selective GABA(A)  $\alpha$ 5 positive allosteric modulators improve cognitive function in aged rats with memory impairment. *Neuropharmacology*. 2013; 64:145–152. [PubMed: 22732440]

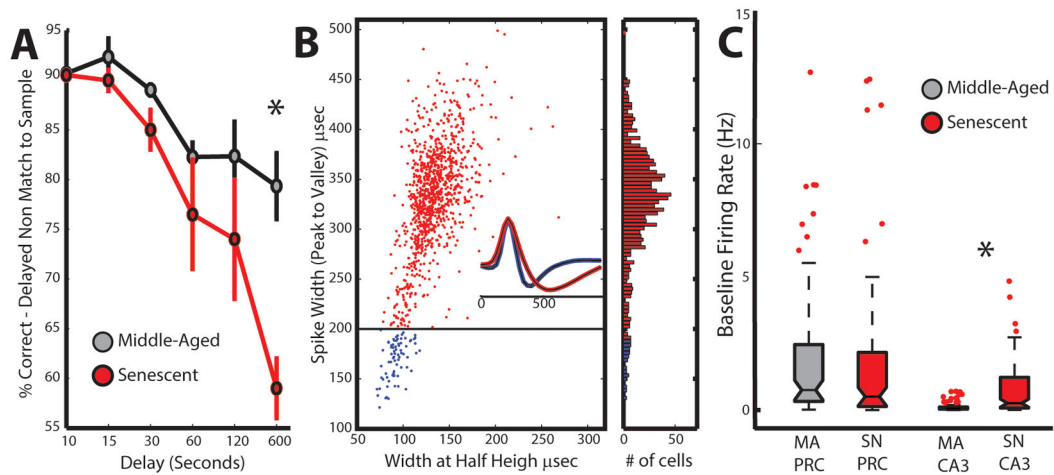


**Figure 1. Behavioral deficits and changes in neuronal excitability**

**A.** Performance on the delayed nonmatching-to-sample task (10, 15, 30, 60, 120 and 600 sec delays) in middle-aged (black) and senescent (red) macaques. Error bars represent standard error of the mean. **B.** Classification of cell type, based on waveform shape. For every recorded single unit (individual points), waveform shape was parameterized into spike width (peak to valley) and spike width at half height. Red dots represent putative principal neurons while blue dots represent putative interneurons. The line at 200  $\mu$ sec represents the boundary between the two cell types. Inset waveforms represent the average waveform drawn from the red and blue distributions and clearly show the shape differences. Histogram to the right represents the frequency of observations of the different neuron types in 10  $\mu$ sec bins. **C.** Region-specific changes in neuronal excitability in medial temporal lobe regions in middle-aged (MA) and senescent (SN) monkeys. Box and whisker plots showing the distribution of baseline firing rates for neurons recorded from the perirhinal cortex and hippocampus region CA3. Box notches represent the median of the distribution, with the top and bottom edges indicating the 25<sup>th</sup> and 75<sup>th</sup> percentile. Whiskers extend to the most extreme points that are not outliers. Outliers are indicated by red dots.

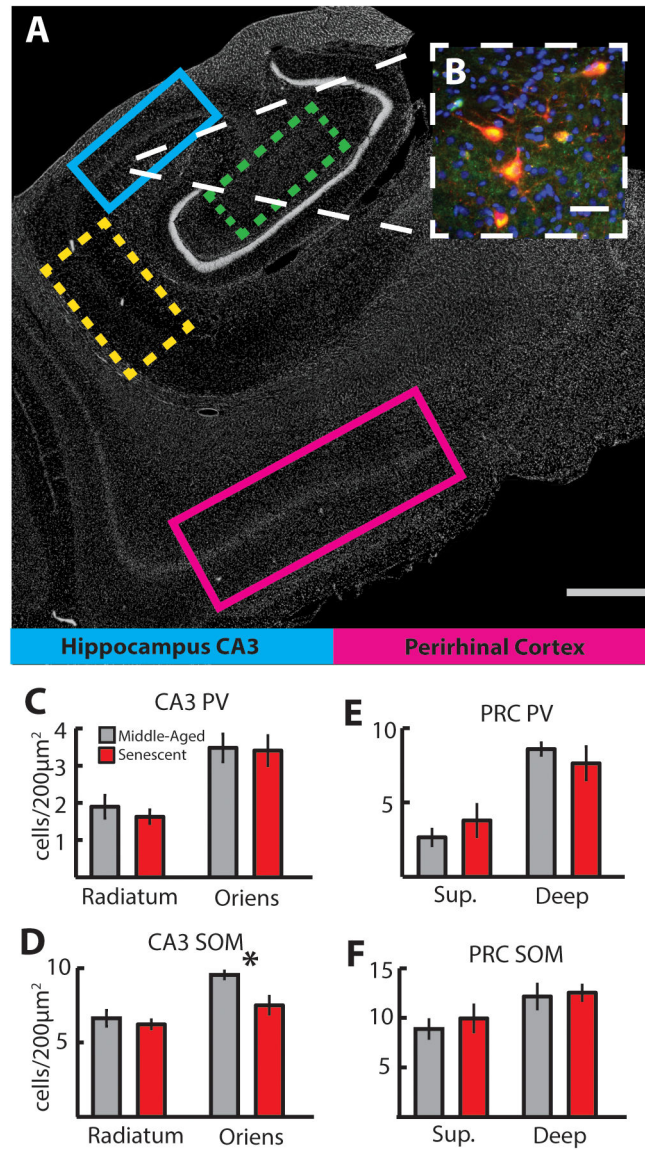


**Figure 2. Regional and cell-type specific reduction in the density of interneurons in senescent animals**

**A.** Coronal cross-section of the macaque temporal lobe showing regions targeted for electrophysiology and immunohistochemistry (blue (CA3) and magenta (PRC), solid boxes) or immunohistochemistry alone (green (Hilus) and yellow (CA1), dashed boxes). Cell bodies stained with DAPI. **B.** High magnification photomicrographs of GAD67-expressing somatostatin (SOM) interneurons in the stratum oriens of the hippocampal CA3 region of a middle aged animal. Red - somatostatin, Blue – DAPI, Green – GAD67. Yellow indicates the co-localization of somatostatin and GAD67 antibodies. We observed no significant differences in the density of parvalbumin-immunopositive interneurons in any layers of the hilus, CA3 (C), CA1 region or PRC (E). There were significant age-dependent differences in the GAD67 expressing somatostatin (SOM)-immunopositive interneurons in stratum oriens of both the CA3 (D) and CA1 regions. There were no significant differences in the

density of SOM neurons in the stratum radiatum of either CA1 (Table 1) or CA3 (**D**). There were no age differences in density of GAD67-expressing somatostatin- or parvalbumin-immunopositive interneurons in any regions of the perirhinal cortex (**F**) or the hilus of the dentate gyrus (Table 1). Scale bar for **A** = 1 mm; for **B** = 40 microns.

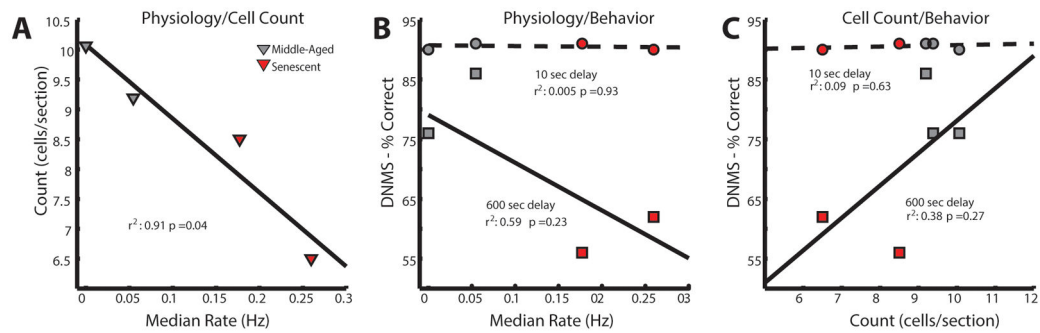


**Figure 3. Relationships between firing rate, interneuron number and performance on the delayed nonmatching-to-sample (DNMS) task**

**A.** Linear regression between median firing rate and median cell count for all animals with CA3 data. Grey-filled symbols = middle-aged animals, red-filled symbols = senescent animals. **B.** Linear regressions between firing rate and percent correct at the 10 second delay on the DNMS task (red/grey circles and dashed line) and the 600 second delay (red/grey squares and solid line). **C.** Linear regressions between somatostatin neuron density and DNMS performance at the 10 second and 600 second delays. Labeling conventions as in **B.**

**Table 1**

**Summary statistics of region-specific histological results**

Summary statistics showing the results of tailed t-test for the hypothesis that there are fewer interneurons in the aged brain than in the young. Data represent the average density of somatostatin and parvalbumin interneurons from middle-aged and senescent animals, and include the mean and standard deviation of within groups, as well as associated test statistics. Only the oriens layer of CA1 and CA3 show significant age-related changes, demonstrating the specificity of the effect.

Somatostatin		Middle Age		Senescent			
Region	Layer	mean	sd	mean	sd	t(df)	p
CA3	Oriens	9.54	0.46	7.53	1.45	t(3) = 2.41	< 0.05
CA3	Radiatum	6.22	0.73	6.63	0.45	t(3) = -0.69	0.73
CA1	Oriens	8.00	0.69	6.01	0.10	t(3) = 3.86	<0.02
CA1	Radiatum	3.83	2.85	3.37	3.26	t(3) = 0.17	0.48
Dentate	Hilus	10.78	2.10	9.96	2.06	t(3) = 0.43	0.35
Perirhinal	Superficial	8.88	1.65	9.94	1.95	t(3) = -0.66	0.72
Perirhinal	Deep	12.15	2.18	12.53	1.11	t(3) = -0.22	0.58

Parvalbumin		Middle Age		Senescent			
Region	Layer	mean	sd	mean	sd	t(df)	p
CA3	Oriens	3.48	0.65	3.41	0.58	t(3) = 0.13	0.45
CA3	Radiatum	1.90	0.54	1.63	0.27	t(3) = 0.64	0.28
CA1	Oriens	2.29	0.51	2.50	0.35	t(3) = -0.49	0.67
CA1	Radiatum	1.02	0.44	1.34	0.40	t(3) = -0.83	0.77
Dentate	Hilus	2.78	1.84	3.04	0.77	t(3) = -0.19	0.57
Perirhinal	Superficial	2.65	0.97	3.78	1.55	t(3) = -1.04	0.81
Perirhinal	Deep	8.58	0.73	7.63	1.59	t(3) = 0.96	0.20